Published in final edited form as:
J Org Chem. 2013 February 1; 78(3): 1208–1215. doi:10.1021/jo302787m.

Origins of Stereoselectivities in Chiral Phosphoric Acid-Catalyzed Allylborations and Propargylations of Aldehydes

Hao Wang[a], **Pankaj Jain**[b], **Jon C. Antilla**[b], and **K. N. Houk**[a,*]

[a]Department of Chemistry and Biochemistry, University of California, Los Angeles, California 90095-1569

[b]Department of Chemistry, University of South Florida, 4202 East Fowler Avenue, Tampa, Florida 33620

Abstract

The chiral BINOL-phosphoric acid catalyzed allylboration and propargylation reactions are studied with density functional theory (B3LYP and B3LYP-D3). Two different models were recently proposed for these reactions by Goodman and our group, respectively. In Goodman's model for allylborations, the catalyst interacts with the boronate pseudo-axial oxygen. By contrast, our model for propargylations predicts that the catalyst interacts with the boronate pseudo-equatorial oxygen. In both models, the phosphoric acid stabilizes the transition state by forming a strong hydrogen bond with the oxygen of the boronate, and is oriented by a formyl hydrogen bond (Goodman model), and by other electrostatic attractions in our model. Both of these models have now been reinvestigated for both allylborations and propargylations. For the most effective catalyst for these reactions, the lowest energy transition state corresponds to Goodman's axial model, while the best transition state leading to minor enantiomer involves the equatorial model. The high enantioselectivity observed with only the bulkiest catalyst arises from the steric interactions between the substrates and the bulky groups on the catalyst, and the resulting necessity for distortion of the catalyst in the disfavored transition state.

Introduction

Asymmetric allylborations of carbonyls are valuable methods in organic synthesis, and occur with high enantioselectivity and diastereoselectivity.[1] The most common method for enantioselective allylboration involves chiral allylboron reagents.[2] However, the preparation of chiral allylboranes and allyl boronates often requires multiple steps and can be challenging. Enantioselective allylborations involving catalytic chiral Lewis acids[3] or Brønsted acids[4] have now been developed. In particular, chiral BINOL-phosphoric acids that have been employed in many other asymmetric reactions[5,6] were recently demonstrated by Antilla to catalyze the enantioselective allylboration reaction between allylboronate **1** and benzaldehyde **2** (Figure 1).[7] The homoallylic alcohol **3** was obtained in 99% yield and 93% ee with catalyst **PA1** bearing bulky 3,3'-substituents. For other aldehydes, including electron-donating aromatic aldehydes, electron-withdrawing aromatic aldehydes and aliphatic aldehydes, the enantioselectivities vary from 73% to 99% ee. The asymmetric propargylation involving allenyl boronic acid pinacol ester **1'** and benzaldehyde **2** was efficiently catalyzed by **PA1** as well, which gave homopropargylic alcohol **3'** in high yield and ee.[8] Catalysts where the Ar groups are less bulky gave much lower ee values.

*houk@chem.ucla.edu. jantilla@usf.edu.

Supporting Information Optimized geometries and energies of all computed species and full authorship of ref 12. This material is available free of charge via the Internet at http://pubs.acs.org.

Using computational methods, we recently proposed a model to explain the enantioselectivities in propargylations.[8] In our model (Figure 2), the phosphoric acid establishes a H-bond with the pseudo-equatorial oxygen of the boronate. The high enantioselectivities observed for **PA1** originate from the larger distortion of the catalyst in the disfavored TS, which is the result of avoiding steric interactions between the allenylboronate methyls and the bulky substituents in the catalyst. At almost the same time, Grayson, Pellegrinet, and Goodman published a computational study of allylboration reactions.[9] In the Goodman et al. work, it was proposed that the hydroxyl group of BINOL phosphoric acid H-bonds to the pseudo-axial oxygen of the boronate, and the phosphoryl oxygen interacts with the aldehyde formyl hydrogen through electrostatic interactions (Figure 2). Due to the large size of the real catalyst, Goodman used ONIOM calculations on the full catalyst **PA1**. The high enantioselectivities were rationalized from the unfavorable steric clash between the pinacol methyl groups and the large alkyl-substituted aromatic group of the catalyst. Despite the differences in the activation modes of two models, steric effects or the resulting distortions of the catalyst are believed to determine the origins of the stereoselectivites in these reactions.

We have reinvestigated the chiral BINOL-phosphoric acid catalyzed allylboration and propargylation reactions using several levels of DFT calculations. In order to study the enantioselectivity of the catalysis, the two different models were evaluated. In addition, we used B3LYP-D3, which includes dispersion energies,[10] to calculate the transition state energies, which may also be important to such systems. Using biphenol (BIPOL)-derived phosphoric acid as the model catalyst, we found that the two competing models are comparable in energy. The diastereomeric TSs involved in allylborations and propargylations for **PA1** were located using fully DFT optimization, and the calculated energies by B3LYP and B3LYP-D3 indicated that both pathways were involved for these systems. Goodman's model with axial coordination has a lower energy for *re*-face attack TS, which leads to the major enantiomeric product. However, in our calculations, for *si*-face attack TS, our model is more stable than Goodman's model, which indicated that the minor enantiomeric TS comes from equatorial coordination of the catalyst.

Results and Discussion

Investigation of the reaction mechanism

The allylboration reaction proceeds via a closed six-membered chairlike transition state.[11] There are three possible coordination positions for the catalyst hydroxyl group: the two boronate oxygens or the aldehyde oxygen. In Goodman's and our models, the phosphoric acid forms a hydrogen bond with the boronate oxygens: either the pseudo-equatorial oxygen (path i: eq), or the pseudo-axial oxygen (path ii: ax). The other plausible mechanistic pathway is the phosphoric acid forming a H-bond with the oxygen of the aldehyde (path iii).

In order to evaluate these different pathways, we first explored transition states where each of the oxygens was protonated. All calculations were performed with the Gaussian 09 package.[12] Geometries were fully optimized in the gas phase and characterized by frequency calculations using B3LYP functional and 6–31G* basis set. Free energies were calculated for each stationary point. The optimized chairlike transition state structure of the uncatalyzed reaction is shown in Figure 4, and the transition states for the three possible sites of protonation are shown in Figure 5 along with their relative Gibbs free energies.

As shown in Figure 5, the pathways involving protonation of boronate oxygens (**TS1**: 0.0 kcal/mol, **TS2**: +3.6 kcal/mol) are more favorable than **TS3** (+4.3 kcal/mol) which involves protonation of the aldehyde oxygen. Protonation of a B–O increases the electrophilicity of the boronate and lowers the activation energy.[13] This finding is in agreement with Hall's

experimental observations[14] and Fujimoto's theoretical studies[15] of similar Lewis acid catalyzed allylboration reactions. Similarly, for propargylations, protonation of boronate oxygens accelerates more than protonation of aldehyde (See Supporting Information).

Model of the phosphoric acid-catalyzed allylboration reaction

The mechanistic studies reported above illustrate that activation of boronate oxygens are more favorable than activation of aldehyde oxygen. This phenomenon is also found in Goodman's model study calculations. In order to better understand the boronate activation pathways, catalyst **PA** without Ar substituents was then employed to study both paths i and ii in more detail. In order to reduce the computational cost, the biphenol (BIPOL)-derived phosphoric acid was initially used as the model instead of the BINOL-derived phosphoric acid. This kind of truncating has previously been justified by Yamanaka, Akiyama and Goodman in their studies.[6] Replacement of the binaphthyl backbone with a smaller biaryl does not significantly alter the geometry around the reaction center.

In both pathways i (eq) and ii (ax), the catalyst interacts with the allylboronate by a single hydrogen bond, and the orientation of the phosphate with respect to the substrate is not fixed. As a result, the remaining parts of the catalyst are conformationally flexible, and there are many possible diastereomeric transition state structures with different orientations of the catalyst. To explore all accessible conformations of the transition states, a conformational search was performed (See Supporting Information: Figure S1).

For pathway i, two low energy transition state structures, **TS4** and **TS4'**, were located for the phosphoric acid-catalyzed allylboration reaction (Figure 6a). In **TS4**, the lowest energy minimum for i, the phosphoryl oxygen was near the six-membered transition state; in **TS4'**, the phosphoryl oxygen is away from the six-membered ring, but next to the boronate methyls. **TS4'** is 1.4 kcal/mol less stable than **TS4**. Since B3LYP may underestimate the aromatic and dispersion interactions in such systems, a method which is expected to treat such interactions more accurately was used to calculate the energy differences between different transition states as well. The energy difference between **TS4** and **TS4'** is calculated to be 2.0 kcal/mol with B3LYP-D3, which includes a dispersion energy correction. For pathway ii, involving H-bonds to the pseudo-axial boronate oxygen, two different diastereomeric transition state conformers, **TS5** and **TS5'** were also found (Figure 6b). **TS5**, in which the phosphoryl oxygen is situated over the six-membered ring TS, was more energetically favorable than **TS5'** by 3.0 kcal/mol. B3LYP-D3 calculation gave an energy difference of 3.5 kcal/mol between **TS5** and **TS5'**. This order of stability between **TS5** and **TS5'** was also observed by Goodman et al.[9]

In order to study the origin of the energy differences between the different transition state conformers, electrostatic potentials were computed. They are shown for the uncatalyzed reaction transition state **TS** in Figure 7. The formyl H, allyl Hs and phenyl Hs are more positive than the Hs on boronate methyls. This indicates that there can be stabilizing electrostatic attractions between the phosphoryl oxygen and those positive Hs. The stabilized interactions between electronegative parts of catalysts and the formyl H has been proposed by Corey before,[16] as well as in Goodman's model. Here, **TS4** was more stable than **TS4'** and **TS5** was more stable than **TS5'**. The extra stabilization of **TS4** and **TS5** comparing to **TS4'** and **TS5'** came from the extra attractive P=O•••H–C interactions, either with the aldehyde H in **TS5** or the phenyl and allyl Hs in **TS4**.

By comparing the most stable TSs in two pathways, **TS4** is calculated to be 0.2 kcal/mol more stable than **TS5** by B3LYP, but 0.7 kcal/mol less stable than **TS5** using B3LYP-D3. In the Goodman et al. work, when buta-1,3-diene-1,4-diol-phosphoric acid, which contains no aromatic rings was used as the model catalyst, the two competing pathways are

differentiated by 2.2 kcal/mol. In our studies, the model catalyst (biphenol-derived phosphoric acid) resembles more the real catalysts in the experiment, and the two different pathways are calculated to be similar in energy. This is likely due to the role of the additional aromatic rings in our model catalyst. The energy differences we calculate are quite small, suggesting that both of them may be involved in the reactions.

On the basis of these investigations, the “two-point binding models” of two different pathways shown in Figure 8 appear to operate for phosphoric acid catalyzed allylborations. The models consider two interactions between the catalyst and the substrates, which provide relative rigidity to the transition state. In what we will refer to as **A** (for axial), which is the same as Goodman's model, the acidic H of the catalyst forms a hydrogen bond with the pseudo-axial oxygen of boronate. In **E** (for equatorial), the hydroxyl group of the catalyst H-bonds to the pseudo-equatorial oxygen of boronate. The second interaction comes from the electrostatic attractions between the phosphoryl oxygen and relatively positive Hs.

Activation barrier for uncatalyzed and catalyzed reactions

Having investigated the mechanism and the model for this chiral phosphoric acid catalyzed allylboration reaction, the issue of the reactivity in the present reaction was then addressed. The uncatalyzed allylboration reaction between allylboronate and benzaldehyde was studied first. The free energy profile is shown in Figure 9. A loose reactant complex **C1** is formed with 7.9 kcal/mol free energy higher than the separated reactants. The activation free energy of the uncatalyzed reaction relative to the separated reactants (**1**+**2**) was calculated to be high, 26.2 kcal/mol (Figure 9). This is consistent with the low reaction rates observed experimentally for the uncatalyzed allylboration reaction.[17]

For the phosphoric acid-catalyzed reaction, in the **E** TS, the catalyst forms a hydrogen bond with the boronate pseudo-equatorial oxygen to afford complex **C2** with 0.6 kcal/mol free energy higher than the separated reactants, as shown in Figure 10. The binding of benzaldehyde on **C2** leads to the reactant complex **C3**. In transition state structure **TS4**, both the forming C-C and B–O bond distances (2.18 Å and 1.51 Å) are shorter than that in the uncatalyzed reaction **TS** (2.23 Å and 1.53 Å), which indicates the electrophilicity of boron is increased by catalyst activation. The calculated activation barrier of the catalyzed reaction relative to the separated reactants (**1**+**2**+catalyst) is 20.2 kcal/mol (Figure 10), 6 kcal/mol lower than the uncatalyzed reaction.

On the other hand, for the **A** TS, the catalyst forms a hydrogen bond with the boronate pseudo-axial oxygen to afford complex **C4**, as shown in Figure 11. The binding of benzaldehyde on **C4** leads to the reactant complex **C5** with 12.8 kcal/mol free energy higher than the separated reactants. In **TS5**, the electrophilicity of boron is also increased by catalyst activation represented by the shorter C-C and B–O bond distances (2.14 Å and 1.50 Å) than that in the uncatalyzed reaction **TS** (2.23 Å and 1.53 Å). And the calculated activation barrier is 20.4 kcal/mol (Figure 11), 5.8 kcal/mol lower than the uncatalyzed reaction.

The two competing pathways give nearly identical energy profiles towards the catalyzed allylboration reactions, which again indicate the possibility that both two pathways are involved in the actual catalyzed reactions.

Origins of Enantioselectivity

The model studies described above indicated that both of the transition states in the two models, **A** and **E**, are likely to be involved in the reactions. To explore the origins of the enantioselectivity of the catalysis, the 3,3'-substituted BIPOL model for the binaphthol

catalyst **PA1** was employed, and both transition states, **A** and **E**, were computed. Catalyst **PA1** bearing the 2,4,6-triisopropylphenyl group on the 3,3'-positions gave high enantioselectivity experimentally. The diastereomeric transition states for *re*-face **(r)** and *si*-face attack **(s)** involving BIPOL model of **PA1** were explored. The transition states involved were fully optimized, in contrast to Goodman's ONIOM calculations for these systems, **TSr1-E**, **TSs1-E** are located for **E** and **TSr1-A**, **TSs1-A** are located for **A**. These are shown in Figure 12.

In the equatorial coordination model **E**, the *re*-face attack **TSr1-E** is predicted to be more favored than the *si*-face attack **TSs1-E** by 2.0 kcal/mol. In the axial coordination model **A**, **TSr1-A** is more stable than **TSs1-A** by 6.1 kcal/mol using B3LYP calculations, which is consistent with Goodman's ONIOM calculations on these two TSs, which gives an energy difference of 6.7 kcal/mol.

In contrast to Goodman's ONIOM calculations that both *re* and *si* TSs are substantially energetically preferable in **A** over **E**, our fully optimized structure energies show that transition states resembling both models contribute to selectivity. That is, using the B3LYP-D3 energetics, the relative rates of reaction via **TSr1-A**, **TSr1-E**, **and TSs1-E** will be 1:0.05:0.001. Use of **A** only predicts far too high selectivity. The energy difference between the most stable *re*-face **(r)** attack transition state **TSr1-A** and the most stable *si*-face **(s)** attack transition state **TSs1-E** is 2.6 kcal/mol by B3LYP, which is in close agreement with the 93% ee observed experimentally. Solvation energy calculations using PCM model with toluene as the solvent does not change the energy difference very much, which gives a number of 3.1 kcal/mol.

Based on these calculations, we compare the two competing models for each enantiomeric TS (*re* or *si*), respectively. In Goodman's paper, the large preference for **A** comes from both steric and electronic factors. In the case of *re*-TSs, our calculations, in agreement with Goodman's results, show **A (TSr1-A)** is more stable than **E (TSr1-E)**. Inspection of the two diastereomeric TSs show they are both free of steric problems by inspecting all the H-H distances; all H-H distances are 2.4 Å or more. The stabilities between two TSs is then perhaps because formyl H-bond strength inside **A (TSr1-A)** is stronger than the electrostatic interactions between phosphoryl oxygen and relative positive Hs in **E (TSr1-E)**.

Our calculations show that **A (TSs1-A)** is much less favorable than **E (TSs1-E)** for *si*-TSs. In our fully optimized TS structures **TSs1-A** and **TSs1-E**, both of them have an almost linear H-bond arrangement. However, **A (TSs1-A)** has a longer H-bond distance (1.65 Å) and corresponding weaker H-bond strength than that in **E (TSs1-E)** (1.59 Å); this is opposite from Goodman's ONIOM calculated structures. We find a steric difference between the two models. Inspection of **A (TSs1-A)** shows that the pinacol group is orientated toward the bulky pocket of the catalyst, and there is one significant steric repulsion between an isopropyl H on the catalyst and a methyl H on the boronate; separated by only 2.15 Å; such steric repulsions are not found in **E (TSs1-E)**. As a result, both electronic and steric factors make **A (TSs1-A)** less favorable than **E (TSs1-E)** in our calculated structures for *si*-TSs.

After comparing the two competing models, it is then necessary to investigate the origins of different stabilities between *re* and *si* TSs in each model, respectively. In **A**, the stabilities between **TSr1-A** and **TSs1-A** are due to steric factors. One significant steric repulsion between isopropyl H on the catalyst and methyl H on the boronate, separated by only 2.15 Å, was found for **TSs1-A**; by contrast **TSr1-A** is free of steric congestion. These steric factors are believed to control the stabilities of two diastereomeric TSs in **A** in Goodman's studies as well.

In **E**, however, as mentioned above, there are no obvious steric differences in the two transition states **TSr1-E** and **TSs1-E**. To gain insights into the origins of the energy difference between **TSr1-E** and **TSs1-E**, the distortion energy (ΔE_d) and interaction energy (ΔE_i) of the transition states were performed. This method has been used previously to understand 1,3-dipolar and Diels-Alder cycloadditions.[18]**TSr1-E** and **TSs1-E** are divided into two parts: catalyst-boronate complex **1A** and the benzaldehyde **1B** (Figure 13b) with the geometries fixed at the transition state geometries. The calculated distortion energy ΔE_d of **1B** in **TSr1-E** (+12.2 kcal/mol) is almost the same as that in **TSs1-E** (+12.3 kcal/mol). There is also no interaction energy ΔE_i difference between **TSr1-E** (−41.3 kcal/mol) and **TSs1-E** (−41.2 kcal/mol) which means all of the stabilizing and destabilizing interactions between **1A** and **1B** in the two TSs are similar. The preference for *re*-facial selectivity is therefore the result of the larger distortion of catalyst-boronate complex **1A** in **TSs1-E**. **1A** is more heavily distorted in **TSs1-E** (+33.9 kcal/mol) than in **TSr1-E** (+32.1 kcal/mol) by 1.8 kcal/mol.

The origins of the differences in distortion energies of **1A** in the two TSs can be visualized from the **1A** geometries, as shown in Figure 13. In Figure 13d, which shows the **1A** structure in **TSs1-E**, the dioxaborolane ring is on the left, and the methyl groups on the dioxaborolane ring and isopropyl groups of catalysts are close to each other (green atoms in Figure 13d). In order to minimize such steric repulsions, the 2,4,6-triisopropylphenyl substituent is rotated around the bond to the BIPOL phenyl core with a dihedral angle of 80°. This is an 8° rotation away from the dihedral angle in the optimized catalyst (72°). Due to the distortion of the catalyst, the green atoms (Figure 13d) are all far away, resulting in no steric repulsions. In other words, the catalyst undergoes conformational changes to avoid unfavorable steric interactions in **TSs1-E**. Figure 13c shows the **1A** structure in **TSr1-E**. Here, the dioxaborolane ring is far from the catalyst, and the dihedral angle between 2,4,6-triisopropylphenyl substituent and the BIPOL core is 72°, the same as the dihedral angle of 72° in the optimized catalyst. The asymmetric induction can be rationalized by differences in distortion energies originating from avoiding the steric interactions between the substrates and the bulky 3,3'-substituents on the catalysts.

After investigating the allylboration reaction, we then reinvestigated the propargylations. The propargylation proceeds via a six-membered cyclic transition state similar to that for allylborations. Once again, the catalyst could activate the reaction by forming a hydrogen bond with either of the boronate oxygens. The transition state structures of propargylation involving the phosphoric acid catalyst **PA1** using both **E** and **A** were studied. As before, diastereomeric transition states **TSr1'-E** and **TSs1'-E** were located for **E**, and **TSr1'-A** and **TSs1'-A** were located for **A** (Figure 14).

As in the allylboration analysis, for *re*-face **(r)** attack, **A** (**TSr1'-A**) is more stable than **E** (**TSr1'-E**) by 2.7 (or 3.5) kcal/mol. For *si*-face **(s)** attack, **A** (**TSs1'-A**) is less stable than **E** (**TSs1'-E**) by 1.3 (or 1.2) kcal/mol. The energy difference between the most stable *re*-face **(r)** attack transition state **TSr1'-A** and the most stable *si*-face **(s)** attack transition state **TSs1'-E** is 4.0 (or 5.1) kcal/mol, overestimating the stereoselectivities as compared to the 74% ee observed experimentally.

Our studies on propargylations still showed that for *re*-TSs, **A** is more favorable; while **E** is more favorable for *si*-TSs. The **A** and **E** transition states leading to *re* attack are both lower in energy than **E** transition state that leads to *si* attack.

In **E**, the calculated distortion energy ΔE_d of benzaldehyde in **TSr1'-E** (+17.4 kcal/mol) is almost the same as that in **TSs1'-E** (+17.5 kcal/mol), so is the interaction energy ΔE_i for the two transition states. The preference for *re*-facial selectivity still comes from the larger

distortion of catalyst-boronate complex in **TSs1'-E**. The catalyst-boronate complex is calculated to be more heavily distorted in **TSs1'-E** (+45.9 kcal/mol) than in **TSr1'-E** (+44.7 kcal/mol) by 1.2 kcal/mol.

The origin of the differences in distortion energies of catalyst-boronate complex in the two TSs is similar to that in the allylboration reaction. In Figure 15b which shows the complex structures in **TSs1'-E**, in order to minimize the steric repulsions between the methyl groups on the dioxaborolane ring and isopropyl groups of catalysts (green atoms in Figure 15b), the 2,4,6-triisopropylphenyl substituent is rotated around the bond to the BIPOL phenyl core with a dihedral angle of 78°. In Figure 15a which shows the catalyst-boronate complex structure in **TSr1'-E**, the dihedral angle between 2,4,6-triisopropylphenyl substituent and the BIPOL core is 74°. The 4° dihedral angle differences of the two complexes accounts for their different distortion energies.

Conclusion

Theoretical calculations have been carried out for the chiral phosphoric acid-catalyzed enantioselective allylboration and propargylation reactions. Transition states with either boronate oxygen hydrogen-bonded to the phosphoric acid were studied. The catalyst is able to activate the boronate by forming a hydrogen bond either with the pseudo-equatorial oxygen (**E**) or the pseudo-axial oxygen (**A**) of the boronate; the phosphoryl oxygen interacts with relatively positive Hs of the substrate through electrostatic attractions, which provides further stabilization of the TS, and a two-point orientation of the catalyst. Pathway **A** is investigated in detail in Goodman's model[9], and our studies focus more on pathway **E** in this paper.

For *re*-face attack, both equatorial and axial coordination gives TSs that are free of steric repulsions, with **A** more favorable than **E.** The relative stability of A is due to the formyl H-bond strength in **A**. For *si*-face attack, to give the minor enantiomer, our calculations showed that **A** is less favorable than **E**. Steric factors make the more crowded **A** less stable than the less crowded **E**.

Calculations show that the enantioselectivity observed experimentally originates from larger distortions of the catalyst in the minor enantiomeric TS, which is the result of the avoidance of the repulsive interactions between the bulky 3,3'-substituents in the catalyst and the substrates. The pinacol boronate methyls have an important role, and these groups could be altered to influence stereoselectivities. These investigations might help direct future enantioselective catalysis development for allylboration and propargylation reactions.

Supplementary Material

Refer to Web version on PubMed Central for supplementary material.

Acknowledgments

This work was supported by the National Science Foundation (CHE 0614591) and National Institute of General Medical Sciences, National Institute of Health (GM36700). Computations were performed on the National Science Foundation Terascale Computing System at the National Center for Supercomputing Applications (NCSA), on the California NanoSystems Institute clusters and UCLA cluster.

References

1. For reviews, see: Denmark SE, Almstead NG. Otera J. Modern Carbonyl Chemistry. 2000; Chapter10:299–402.Wiley-VCHWeinheim. Chemler SR, Roush WR. Otera J. Modern Carbonyl Chemistry. 2000; Chapter 11:403–490.Wiley-VCHWeinheim. Yamamoto Y, Asao N. Chem. Rev.

1993; 93:2207–2293.. Denmark SE, Fu J. Chem. Rev. 2003; 103:2763–2793. [PubMed: 12914480] . Lachance H, Hall DG. Org. React. 2008; 73:1.. Roush WR. Trost BM. Comprehensive Organic Synthesis. 1991; Vol. 2:1.Pergamon PressOxford, U.K.. Yus M, González-Gómez JC, Foubelo F. Chem. Rev. 2011; 111:7774–7854. [PubMed: 21923136] .

2. (a) Roush WR, Walts AE, Hoong LK. J. Am. Chem. Soc. 1985; 107:8186–8190.(b) Roush WR, Palkowitz AD, Ando K. J. Am. Chem. Soc. 1990; 112:6348–6359.(c) Brown HC, Bhat KS, Randad RS. J. Org. Chem. 1989; 54:1570–1576.(d) Brown HC, Randad RS, Bhat KS, Zaidlewicz M, Racherla US. J. Am. Chem. Soc. 1990; 112:2389–2392.(e) Corey EJ, Yu C-M, Lee D-H. J. Am. Chem. Soc. 1990; 112:878–879.(f) Gonzalez AZ, Roman IG, Alicea E, Canales E, Soderquist JA. J. Am. Chem. Soc. 2009; 131:1269–1273. [PubMed: 19117388] (g) Burgos CH, Canales E, Matos K, Soderquist JA. J. Am. Chem. Soc. 2005; 127:8044–8049. [PubMed: 15926828] (h) Wu TR, Shen L, Chong JM. Org. Lett. 2004; 6:2701–2704. [PubMed: 15281748] (i) Lachance H, Lu X, Gravel M, Hall DG. J. Am. Chem. Soc. 2003; 125:10160–10161. [PubMed: 12926924] (j) Chen M, Handa M, Roush WR. J. Am. Chem. Soc. 2009; 131:14602–14603. [PubMed: 19778012] (k) Althaus M, Mahmood A, Suarez JR, Thomas SP, Aggarwal VK. J. Am. Chem. Soc. 2010; 132:4025–4028. [PubMed: 20192266]

3. (a) Kennedy JWJ, Hall DG. J. Am. Chem. Soc. 2002; 124:11586–11587. [PubMed: 12296710] (b) Lachance H, Xu M, Gravel M, Hall DG. J. Am. Chem. Soc. 2003; 125:10160–10161. [PubMed: 12926924] (c) Hall DG. Synlett. 2007:1644–1655.(d) Kennedy JWJ, Hall DG. J. Org. Chem. 2004; 69:4412–4428. [PubMed: 15202896] (e) Rauniyar V, Hall DG. J. Am. Chem. Soc. 2004; 126:4518–4519. [PubMed: 15070360] (f) Carosi L, Lachance H, Hall DG. Tetrahedron. 2005; 46:8981–8985. (g) Rauniyar V, Zhai H, Hall DG. J. Am. Chem. Soc. 2008; 130:8481–8490. [PubMed: 18540580] (h) Rauniyar V, Hall DG. J. Org. Chem. 2009; 74:4236–4241. [PubMed: 19422213] (i) Ishiyama T, Ahiko T.-a. Miyaura N. J. Am. Chem. Soc. 2002; 124:12414–12415. [PubMed: 12381174] (j) Wada R, Oisaki K, Kanai M, Shibasaki M. J. Am. Chem. Soc. 2004; 126:8910–8911. [PubMed: 15264818]

4. (a) Yu SH, Ferguson MJ, McDonald R, Hall DG. J. Am. Chem. Soc. 2005; 127:12808–12809. [PubMed: 16159268] (b) Rauniyar V, Hall DG. Angew. Chem., Int. Ed. 2006; 45:2426–2428.(c) Elford TG, Arimura Y, Yu SH, Hall DG. J. Org. Chem. 2007; 72:1276–1284. [PubMed: 17288375] (d) Rauniyar V, Zhai H, Hall DG. J. Am. Chem. Soc. 2008; 130:8481–8490. [PubMed: 18540580]

5. For reviews, see: Akiyama T. Chem. Rev. 2007; 107:5744–5758. [PubMed: 17983247] . Terada M. Chem. Commun. 2008:4097–4112.. Brunel JM. Chem. Rev. 2005; 105:857–897. [PubMed: 15755079] . Chen Y, Yekta S, Yudin AK. Chem. Rev. 2003; 103:3155–3211. [PubMed: 12914495] . Akiyama T, Itoh J, Fuchibe K. Adv. Synth. Catal. 2006; 348:999–1010.. Connon SJ. Angew. Chem., Int. Ed. 2006; 45:3909–3912.. Rueping M, Kuenkel A, Atodiresei I. Chem. Soc. Rev. 2011; 40:4539–4549. [PubMed: 21614342] . Zamfir A, Schenker S, Freund M, Tsogoeva SB. Org. Biomol. Chem. 2010; 8:5262–5276. [PubMed: 20820680] .

6. For theoretical studies on the chiral phosphoric acid catalysis, see: Yamanaka M, Itoh J, Fuchibe K, Akiyama T. J. Am. Chem. Soc. 2007; 129:6756–6764. [PubMed: 17477527] . Simo'n L, Goodman JM. J. Am. Chem. Soc. 2008; 130:8741–8747. [PubMed: 18543923] . Simo'n L, Goodman JM. J. Am. Chem. Soc. 2009; 131:4070–4077. [PubMed: 19249818] . Simo'n L, Goodman JM. J. Org. Chem. 2010; 75:589–597. [PubMed: 20039624] . Simo'n L, Goodman JM. J. Org. Chem. 2011; 76:1775–1788. [PubMed: 21309597] . Marcelli T, Hammar P, Himo F. Chem. Eur. J. 2008; 14:8562–8571. [PubMed: 18683177] . Akiyama T, Morita H, Bachu P, Mori K, Yamanaka M, Hirata T. Tetrahedron. 2009; 65:4950–4956.. Shi F-Q, Song B-A. Org. Biom. Chem. 2009; 7:1292–1298.. Yamanaka M, Hirata T. J. Org. Chem. 2009; 74:3266–3271. [PubMed: 19388712] . Gridnev ID, Kouchi M, Sorimachi K, Terada M. Tetrahedron Lett. 2007; 48:497–500..

7. Jain P, Antilla JC. J. Am. Chem. Soc. 2010; 132:11884–11886. [PubMed: 20690662]

8. Jain P, Wang H, Houk KN, Antilla JC. Angew. Chem., Int. Ed. 2012; 124:1420–1423.

9. Grayson MN, Pellegrinet SC, Goodman JM. J. Am. Chem. Soc. 2012; 134:2716–2722. [PubMed: 22239113]

10. (a)For dispersion correction, see:Grimme S. J. Comput. Chem. 2006; 27:1787–1799. [PubMed: 16955487] . Grimme S, Antony J, Ehrlich S, Krieg H. J. Chem. Phys. 2010; 132:154104. [PubMed: 20423165] . For application of dispersion corrected DFT in computational chemistry, see: McMullin CL, Jover J, Harvey JN, Fey N. Dalton Trans. 2010; 39:10833–10836. [PubMed:

20963224] . Antoline JE, Krenske EH, Lohse AG, Houk KN, Hsung RP. J. Am. Chem. Soc. 2011; 133:14443–14451. [PubMed: 21851070] .

11. (a) Li Y, Houk KN. J. Am. Chem. Soc. 1989; 111:1236–1240.(b) Gung BW, Xue X, Roush WR. J. Am. Chem. Soc. 2002; 124:10692–10697. [PubMed: 12207523]
12. Frisch, MJ., et al. Gaussian 09. Gaussian, Inc.; Wallingford, CT: 2010. revision B.01
13. (a) Omoto K, Fujimoto H. J. Org. Chem. 1998; 63:8331–8336.(b) Brown HC, Racherla US, Pellechia PJ. J. Org. Chem. 1990; 55:1868–1874.
14. Rauniyar V, Hall DG. J. Am. Chem. Soc. 2004; 126:4518–4519. [PubMed: 15070360]
15. Sakata K, Fujimoto H. J. Am. Chem. Soc. 2008; 130:12519–12526. [PubMed: 18712868]
16. (a) Corey EJ, Rohde JJ, Fischer A, Azimioara MD. Tetrahedron Lett. 1997; 38:33–36.(b) Corey EJ, Rohde JJ. Tetrahedron Lett. 1997; 38:37–40.(c) Corey EJ, David BS, Thomas WL. Tetrahedron Lett. 1997; 38:1699–1702.
17. Ishiyama T, Ahiko T, Miyaura N. J. Am. Chem. Soc. 2002; 124:12414–12415. [PubMed: 12381174]
18. (a) Ess DH, Houk KN. J. Am. Chem. Soc. 2008; 130:10187–10198. [PubMed: 18613669] (b) Ess DH, Houk KN. J. Am. Chem. Soc. 2007; 129:10646–10647. [PubMed: 17685614] (c) Ess DH, Jones GO, Houk KN. Org. Lett. 2008; 10:1633–1636. [PubMed: 18363405] (d) Garcl'a JI, Martl'nez-Merino V, Mayoral JA, Salvatella L. J. Am. Chem. Soc. 1998; 120:2415–2420.(e) Sbai A, Branchadell V, Ortun~o RM, Oliva A. J. Org. Chem. 1997; 62:3049–3054. [PubMed: 11671684]

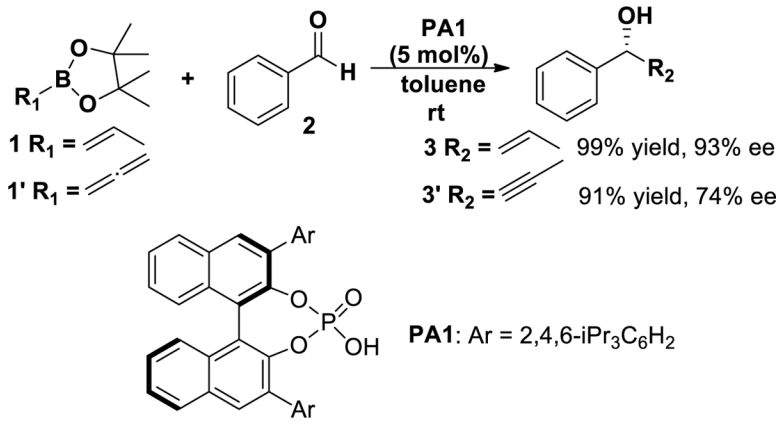

Figure 1.
Chiral phosphoric acid-catalyzed allylborations and propargylations of benzaldehyde.

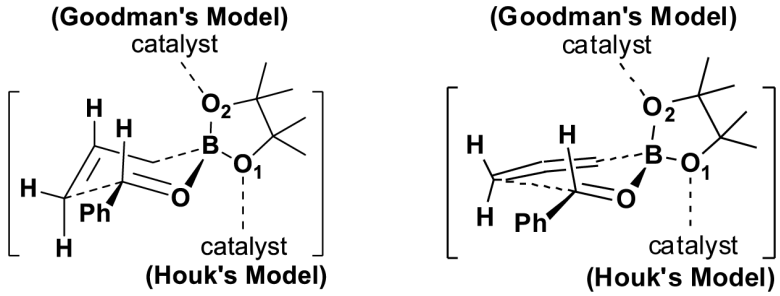

Figure 2.
Two models for the chiral phosphoric acid-catalyzed allylborations and propargylations of benzaldehyde.

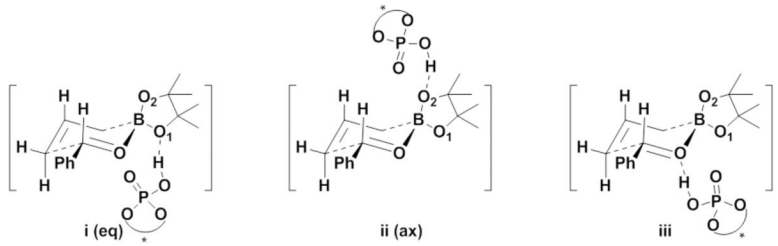

Figure 3.
Three possible sites of coordination in the phosphoric acid-catalyzed allylboration reaction.

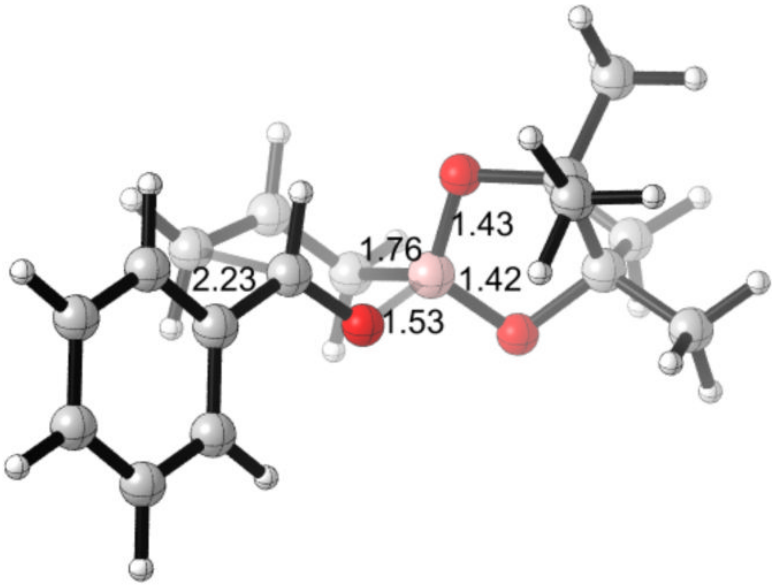

Figure 4.
Optimized transition state of the uncatalyzed allylboration of benzaldehyde at the B3LYP/6–31G* level of theory.

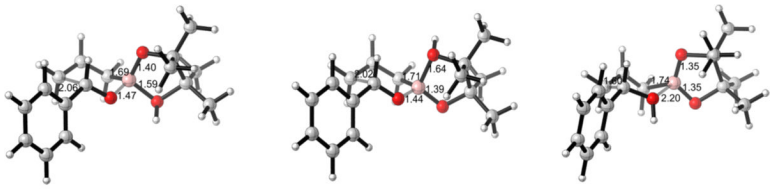

TS1 (0.0) **TS2** (+3.6) **TS3** (+4.3)

Figure 5.
Optimized transition states of different mechanisms at the B3LYP/6–31G* level of theory. Bond lengths are given in Å. Relative free energies (kcal/mol) are shown in parentheses.

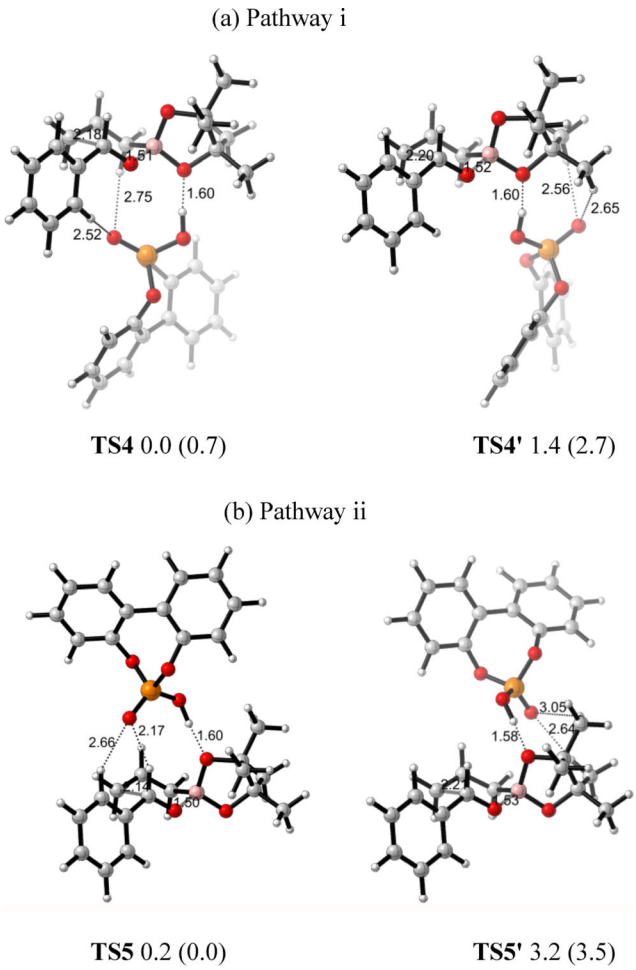

Figure 6.

Optimized transition state structures of (a) **TS4**, **TS4'** in pathway i (eq) and (b) **TS5**, **TS5'** in pathway ii (ax) at the B3LYP/6–31G* level of theory. Bond lengths are given in Å. Values next to each structure are energies relative to **TS4** in kcal/mol. Values in parentheses are energies relative to **TS5** calculated by B3LYP-D3.

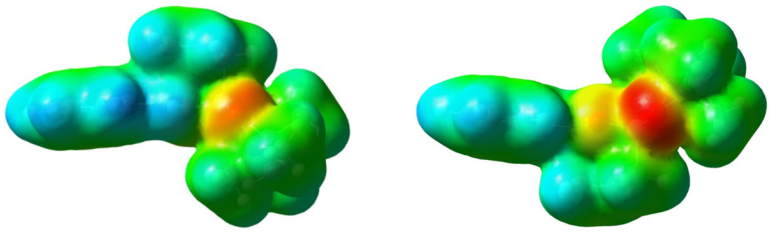

Figure 7.
Top and bottom view of electrostatic potential of **TS** from Figure 4. Red: negative ESP; Blue: positive ESP; Green: neutral.

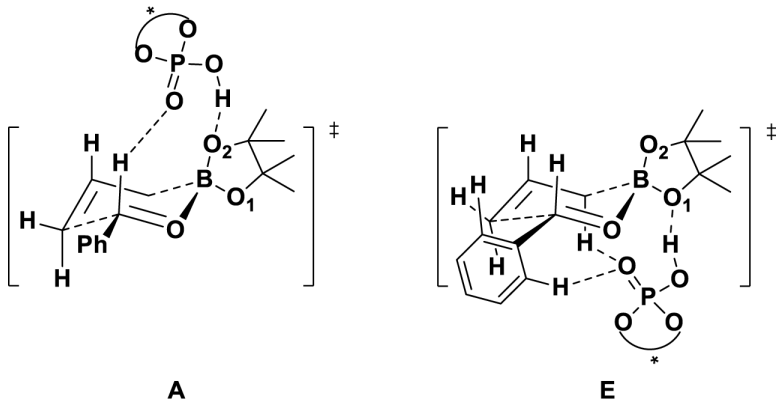

Figure 8.
Models for the phosphoric acid-catalyzed allylboration reaction.

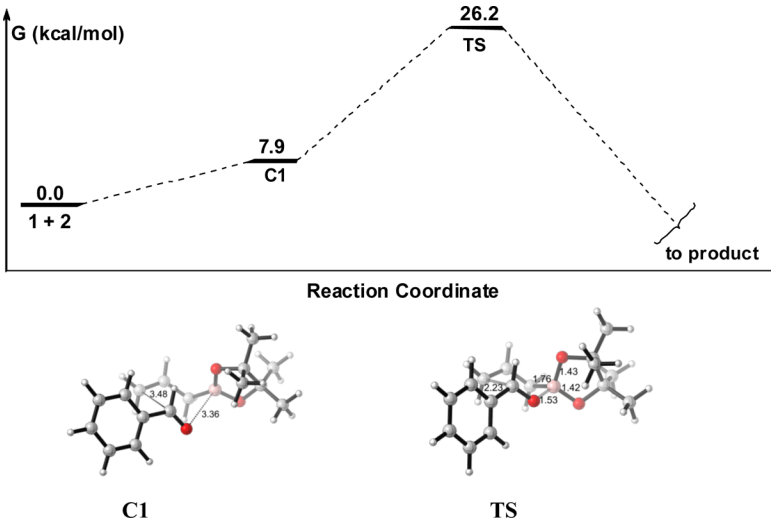

Figure 9.

Reaction profile for the uncatalyzed allylboration reaction of **1** with **2** by B3LYP. Free energies relative the reactants in the gas phase. Optimized geometries of the complexes **C1** and transition state **TS** are shown below the reaction profile.

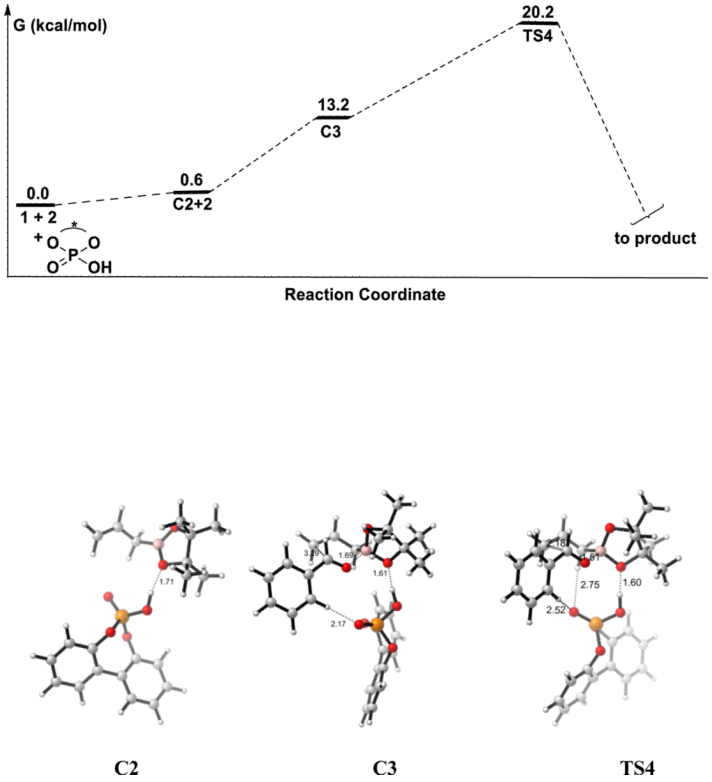

Figure 10.

Reaction profiles for the allylboration reaction of **1** with **2** catalyzed by chiral phosphoric acid using **E** by B3LYP. Free energies relative the reactants in the gas phase. Optimized geometries of the complexes **C2**, **C3** and transition state **TS4** are shown below the reaction profile.

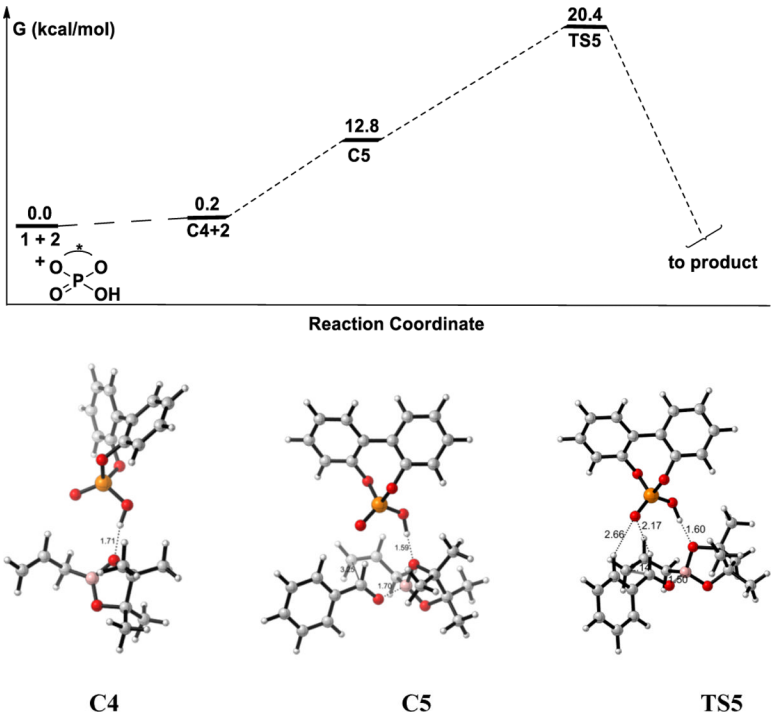

Figure 11.

Reaction profiles for the allylboration reaction of **1** with **2** catalyzed by chiral phosphoric acid using **A** by B3LYP. Free energies relative the reactants in the gas phase. Optimized geometries of the complexes **C4**, **C5** and transition state **TS5** are shown below the reaction profile.

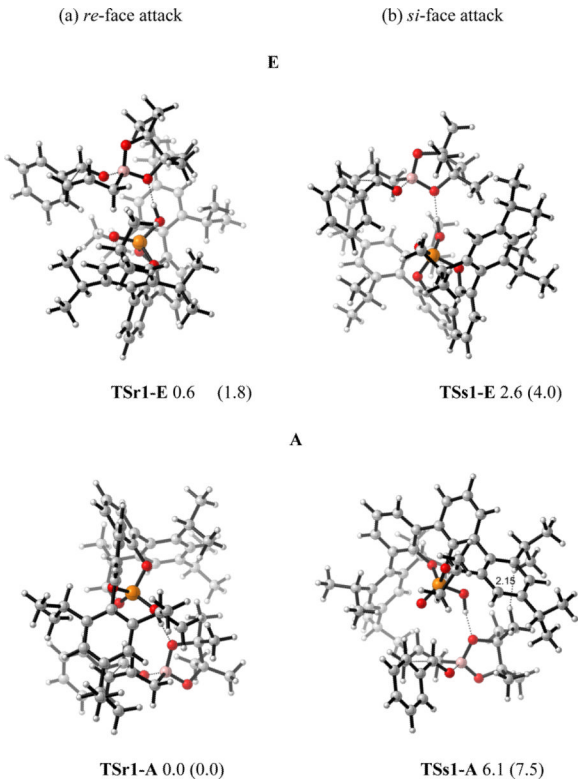

Figure 12.

Optimized structures of **TSr1-E** and **TSs1-E** for **E, TSr1-A** and **TSs1-A** for **A**. Values next to each structure are energies relative to **TSr1-A** in kcal/mol. Values enclosed in parentheses are energies relative to **TSr1-A** calculated by B3LYP-D3.

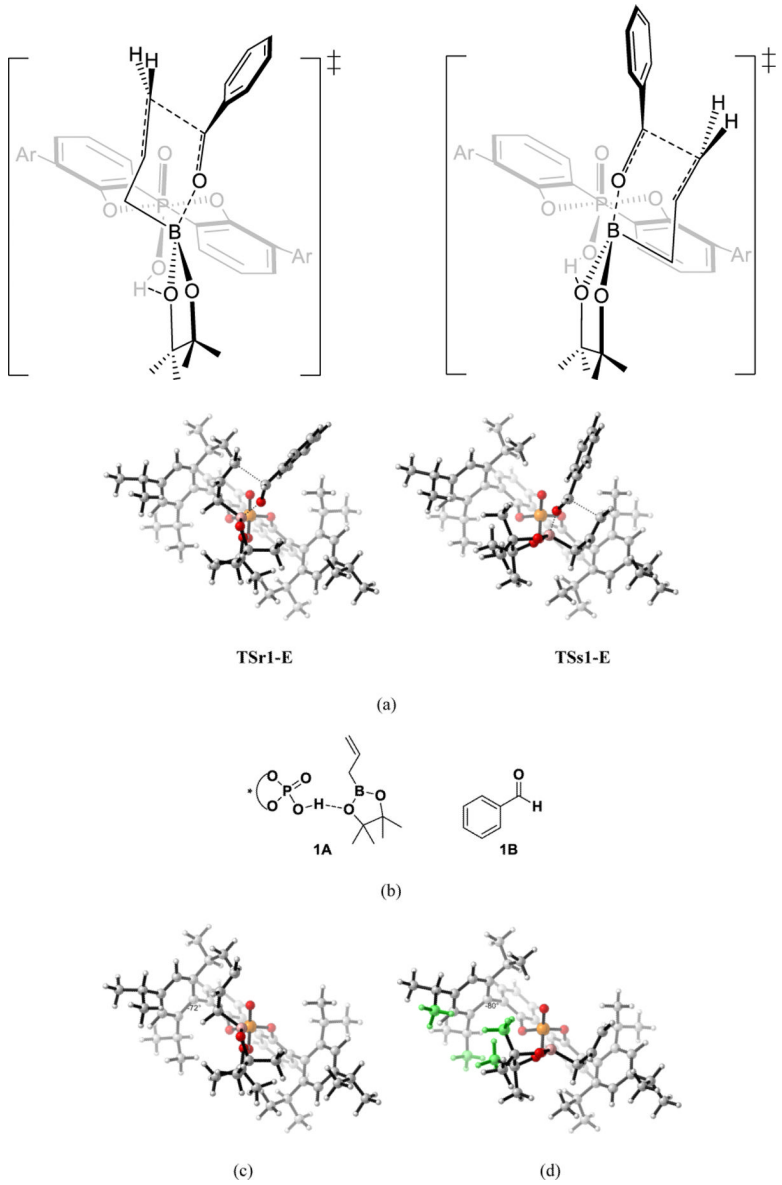

Figure 13.

(a) Side view of **TSr1-E** and **TSs1-E**. (b) Structures of **1A** and **1B**. (c) 3D structures of **1A** in **TSr1-E**. (d) 3D structures of **1A** in **TSs1-E**.

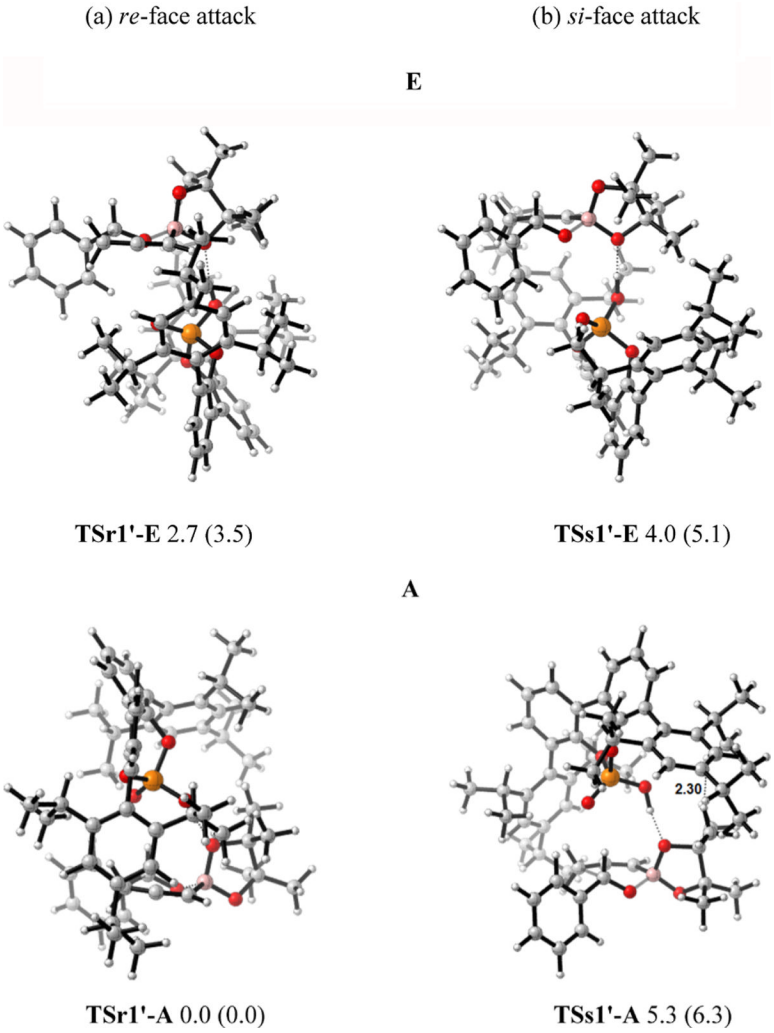

Figure 14.

Optimized structures of **TSr1'-E** and **TSs1'-E** for E, **TSr1'-A** and **TSs1'-A** for **A**. Values next to each structure are energies relative to **TSr1'-A** in kcal/mol. Values enclosed in parentheses are energies relative to **TSr1'-A** calculated by B3LYP-D3.

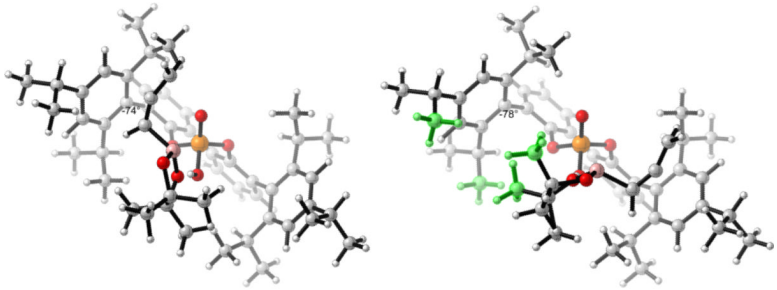

(a) (b)

Figure 15.

(a) 3D structure of **TSr1'-E** without the benzaldehyde. (b) 3D structure of **TSs1'-E** without the benzaldehyde.